J Therm Anal Calorim (2010) 102:983–988
DOI 10.1007/s10973-010-0860-3

Intercalation of water and guest molecules within Ca^{2+}–Montmorillonite

DSC studies in low temperature range

N. A. Halim · Z. A. Ibrahim · A. B. Ahmad

Received: 1 March 2010 / Accepted: 27 April 2010 / Published online: 11 May 2010

Abstract The high potential for intercalations by water and various guest molecules is induced by the exchangeable cation inside Ca^{2+}–Montmorillonite gallery. XRD peak for Mon at $2\theta = 6.04°$ ($d_{001} = 1.462$ nm) shows the structural effect on the clay gallery influenced by the intercalated water layers. Further increases in the gallery height are observed with the intercalation of octadecyl ammonium cations in OMON ($d_{001} = 1.840$ nm) and ENR-50 matrix chains in CENR-50 ($d_{001} = 1.954$ nm). DSC studies on the other hand reveal the thermal behaviors of intercalated molecules that are linked to the exchangeable cations. The endothermic of Ca^{2+}–Montmorillonite ($H_{Mon} = 356.3$ J/g) in low temperature range (30–100 °C) indicates the removal of free water and hydrogen bonded water molecules, while the endothermic around 150 °C is related to the induced skeletal layer of water within Ca^{2+}–Montmorillonite. The OMON endothermic ($H_{OMON} = 47.0$ J/g, $T_m = 36.94$ °C) tells that cation exchange had modified the water structures and content inside the renewed clay. The intercalation of ENR-50 chains into OMON gallery reveals two endothermic with the T_{m1} and T_{m2} are at 86.24 and 113.80 °C, respectively. These T_ms confirm that the alkyl chain segment on octadecyl ammonium cation occupy the OMON interlayer space.

Keywords Montmorillonite modifier molecule · DSC · XRD · FTIR · Intercalation and water layer

N. A. Halim (✉) · Z. A. Ibrahim · A. B. Ahmad
Department of Physics, University of Malaya, 50603 Kuala Lumpur, Malaysia
e-mail: norhanaah@gmail.com

Introduction

Montmorillonite (Mon) like most of the clay minerals belongs to the class of layered silicate or phylosilicate because of their structural framework. It is basically composed of layers comprising silica and alumina sheets that are combined in varying proportion and stacked on top of each other in a certain way. Clay minerals from smectite group, for example, are produced from condensation of 2:1 ratio of tetrahedral silica and octahedral alumina sheet that give rise to a trimorphic or three-sheet mineral [1, 2]. Montmorillonite is the most significant and widely used clay mineral from this smectite group [3, 4]. According to Hoffman [1], isomorphous substitution on the montmorillonite layer structure results in its high negative surface charge. The positively charged hydrable counterions (exchangeable cations) within the clay interlayer act to balance the surface charge.

The presence of exchangeable cations in montmorillonite contributes to its high swelling capacity, especially when immersed in water. This property exposes large active area that allows huge range, both in number and variety of guest molecules to intercalate into the clay interlayer. The intercalation of organic molecules such as alkyl ammonium modifies montmorillonite into an organoclay mineral. The modification by exchanging the original cation for organocation in montmorillonite gallery changes its organophobic property to become organophilic. The great advantage of organically modified montmorillonite (OMON) has many industrial applications, such as in removing oil from water and in polymer composite fabrication [5, 6].

Polymer–organoclay composite attracts a lot of attention in material studies owing to the improved properties shown by such composite; for example, it poses superior mechanical

property, better chemical and heat resistance, as well as reduced gas permeability that presents various useful applications [7–9]. The intercalation of modifier molecules or matrix chains affects the layered structure of OMON. The clay interlayer height or basal spacing d_{001} will become increased to accommodate the guest molecules. The effect can be seen in X-ray diffraction (XRD) pattern, where the shifted d_{001} peak of montmorillonite indicate the changes in the interlayer height. Using the Bragg's equation, the changes in basal spacing d_{001} can be estimated. This technique became the fundamental tool in demonstrating the effect of intercalation [6–8].

In this study, thermal analysis via the differential scanning calorimetry (DSC) technique were carried out on Ca^{2+}–montmorillonite, octadecylamine (ODA, modifier compound), OMON, and polymer–OMON composite. From the studies, it is obvious that the thermal response of OMON also demonstrates the effect of intercalation that hides the modifier molecules within the clay gallery.

Experimental

Materials

Ca^{2+}–Montmorillonite (Ca^{2+}–Mon) SWy2 used in this study was obtained from the Clay Mineral Society Repository in Wyoming and supplied by the University of Missouri, USA. The exchangeable cation in between Ca^{2+} and Mon layers is represented by the cation exchange capacity (CEC) of 76.4 meq/100 g. Octadecylamine and hydrochloride acid used in organoclay modification were purchased from Fluka (Malaysia). The modified Epoxidized Natural Rubber (ENR-50) was supplied by the Rubber Research Institute of Malaysia, *RRIM*. Toluene (Merck Co.) was employed as the reagent for this rubber. All the materials were used as received without further purification.

Sample preparation

Organically modified Ca^{2+}–Montmorillonite

8.0 g of Ca^{2+}–Mon was dispersed into 500 mL of distilled water at a temperature of 80 °C using a homogenizer. 3.1 g of ODA was dissolved in 200 mL of distilled water (80 °C) together with 1.2 mL of concentrated hydrochloric acid. The mixture was then slowly poured into the Ca^{2+}–Mon–water solution under vigorous stirring for 5 min. The obtained white precipitate was then collected on a white cloth filter and washed using distilled water (80 °C) repeatedly for five times. Finally, the organophilic Ca^{2+}–Mon (OMON) precipitate was left to dry at ambient temperature for a few days.

ENR-50–OMON (CENR-50) composite

ENR-50 rubber as received was in big chunk, and it was cut into smaller pieces (1 mm × 1 mm × 5 mm) for sample preparation. 14 g of ENR-50 was combined with 150 mL of toluene in a glass beaker. It was left to swell with constant stirrings using a magnetic stirrer for 3 days at room temperature. 5 mL of acetic acid was also included into the mixture to assist the swelling process of the ENR-50 rubber. 6 g of OMON was then added into the mixture to prepare the ENR-50–OMON (CENR-50) composite. After 3 days of stirring, the mix was poured into a glass container and left to dry for one week at room temperature.

Characterization

The X-ray diffraction (XRD) measurement was done using a Siemens XRD diffractometer model D5000, where nickel-filtered Cu Kα radiation ($\lambda = 0.154$ nm) was employed with the applied voltage of 40 kV and a current of 40 mA. The XRD patterns were recorded with a step size of 0.02° from $2\theta = 2°$ to $2\theta = 50°$. The changes in basal spacing d_{001} of Montmorillonite particles can be detected by analyzing the XRD data, which was carried out based on the Bragg's law [10].

$$nk\lambda = 2d \sin\theta,$$

where n = an integer, k = constant (generally = 0.9) m, λ = wavelength (0.1541 nm), d = basal spacing (nm), and θ = the diffraction angle (°).

The Rheometric Scientific DSC Gold with a heat flux system was used for the differential scanning calorimetry (DSC) measurement. The measurement was performed on samples at the heating rate of 10 °C/min, after quenching the temperature down to −100 °C using liquid nitrogen. Thermal responses from the scans were recorded within the temperature ranging from −100 to 200 °C. The heat fusion of an endothermic can be estimated from the heat flow versus temperature plot using the equation [11],

$$\text{Heat fusion,} \quad H = \frac{1}{\beta}\int \frac{\mathrm{d}H}{\mathrm{d}T}\mathrm{d}T$$

where the heating rate, $\beta = \frac{\mathrm{d}T}{\mathrm{d}t}$ and T = temperature.

Infra-red spectroscopy was carried out on several samples using the FT-IR spectrometer Nicollet Magna-IR 5508 at a spectral resolution of 2 cm^{-1}. The solid clay minerals were pressed in potassium bromide (KBr) to form a disk for the FT-IR samples.

Result and discussion

X-ray diffraction

Figure 1 shows the diffraction pattern from $2\theta = 2°$ to 30° produced by the XRD scan on ODA. Various sharp peaks observed indicate the presence of polymer crystalline structures within the material. Similar sharp peaks are also seen in Fig. 2 at the $2\theta = 26.68°$ and 27.72°, while the other three peaks at 6.04°, 19.80°, and 28.40° are comparatively wide and weak. These peaks represent the crystallite structures within the inorganic Ca^{2+}–Mon clay mineral. The important characteristic peak, however, is given by the peak at $2\theta = 6.04°$ that is related to (*001*) plane. It gives the basal spacing, $d_{001} = 1.462 \pm 0.001$ nm for the Ca^{2+}–Mon interlayer. The measured basal spacing d_{001} indicates that the hydration characteristic of Ca^{2+}–Mon is controlled by the Ca^{2+} cations in the clay gallery. The formation of two molecular water layers in the presence of polyvalent Ca^{2+} cations give the gallery heights of around 1.45–1.55 nm [2]. In the FTIR spectrum, Fig. 3, the presence of interlayer water within Ca^{2+}–Mon is shown by the bands around 1,651 cm^{-1} (∂HOH) and 3,438 cm^{-1} (*ν*OH) [12].

The modification carried out on Ca^{2+}–Mon into OMON involved the replacement of Ca^{2+} cations with octadecylammonium ($C_{18}H_{37}NH_3^+$) cations in the clay gallery. As a result, the characteristic (*001*) peak is shifted to $2\theta = 4.80°$ in Fig. 4, which gives the new basal spacing, d_{001} of about 1.840 ± 0.001 nm. The increment in d_{001} spacing about 0.378 nm demonstrates the effect of intercalation by the modifier molecules, which had increased the OMON gallery height. Organic molecules within OMON gallery facilitate organic matrix chains to penetrate the clay interlayer. The effect is demonstrated in Fig. 4, where the intercalation of ENR-50 matrix chains shifted (*001*) peak from $2\theta = 4.80°$–4.52°. It gives a new d_{001} spacing $= 1.954 \pm 0.001$ nm, which indicates an increase of about 0.114 nm in the OMON gallery height within the CENR-50 composite.

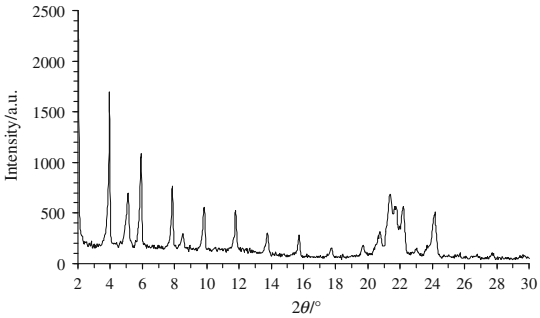

Fig. 1 XRD pattern of octadecylamine (ODA)

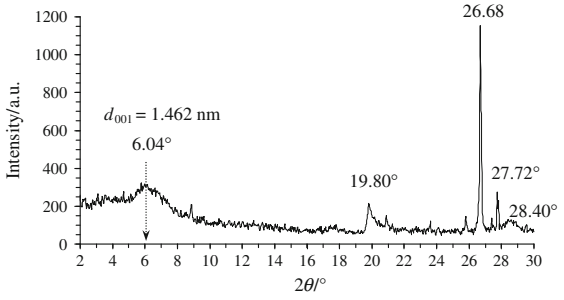

Fig. 2 XRD diffraction pattern of Ca^{2+}–Montmorillonite (Ca^{2+}–Mon)

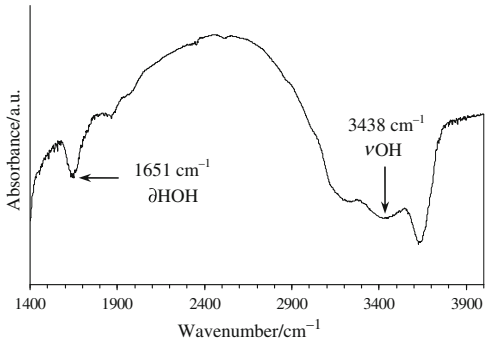

Fig. 3 FTIR spectrum of Ca^{2+}–Montmorillonite shows the hydroxyl bending (1,651 cm^{-1}) and stretching (3,438 cm^{-1}) bands

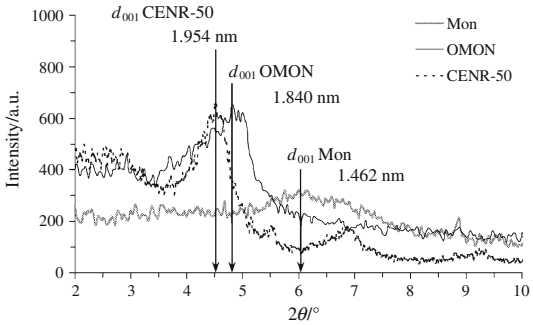

Fig. 4 XRD patterns of Ca^{2+}–Montmorillonite, OMON, and CENR-50 composite

Differential scanning calorimetry

Octadecylamine

Figure 5 shows the thermal response of ODA with the two endothermics at 62.77 and 89.53 °C, which are assigned as T_{m1} and T_{m2}, respectively. The calculated heat fusions are $H_1 = 359.0 \pm 0.1$ J/g and $H_2 = 104.2 \pm 0.1$ J/g. These results indicate the melting of polymer crystallite structures in ODA. The appearance of T_{m2} could be the indicator of a multi-stage mode in the melting process at T_{m1} [13].

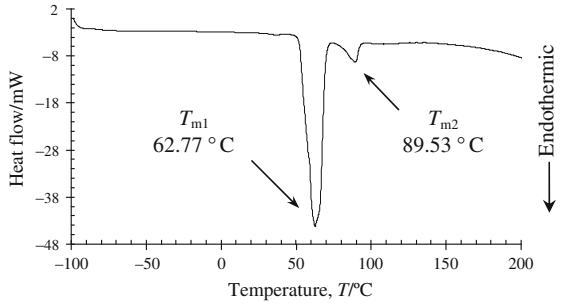

Fig. 5 DSC curve of octadecylamine (ODA)

However, the lack of exothermic peak in between these two endothermics suggests that the T_{m2} actually demonstrates the melting process of different crystallite structures. The T_ms thus indicates a variety of crystalline structures in ODA, which is consistent with various XRD peaks observed in Fig. 1.

Ca^{2+}–Montmorillonite

Differential scanning calorimetry (DSC) profile for Ca^{2+}–Mon in Fig. 6 demonstrates a big and wide endothermic with the T_m around 57.92 °C. The endothermic (H_{Mon} = 356.3 ± 0.1 J/g) that appears in the range of 30–100 °C indicates the removal of free water molecules, which are intercalated in between Ca^{2+} and Mon layers as illustrated in Fig. 7 [1, 2]. However, Bray's et al. [14] studies on Ca^{2+}–Mon had demonstrated significant reduction in d_{001} spacing from 1.5 to 1.25 nm within the temperature range.

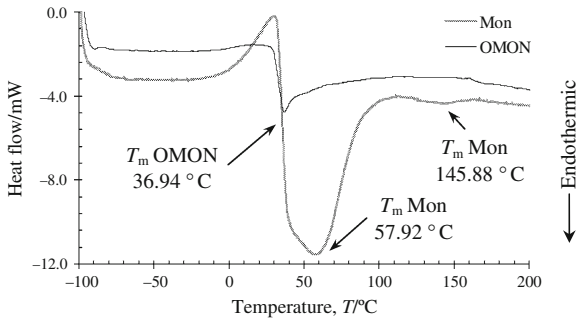

Fig. 6 DSC curve of Ca^{2+}–Mon and OMON clay minerals

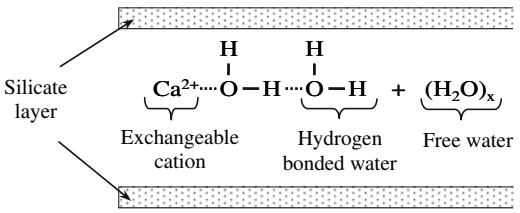

Fig. 7 Schematic diagram of water structure within Ca^{2+}–Mon interlayer space [1]

Table 1 The effects of temperature on water layer and basal spacing d_{001} of Ca^{2+}–Mon clay mineral

Temperature, *T*/°C	Basal spacing d_{001}/nm*	Water layer*
30	1.50	2 layer
150	1.17	1 layer
300	1.03	0 layer

* Bray et al. [14]

From Table 1, d_{001} = 1.5 nm is associated to two water molecule layers state and the decreased d_{001} indicates the distorted interlayer water structures. It thus suggests that water removal contributed to the endothermic also involved the hydrogen bonded water molecules. Further heating had caused the small endothermic with its T_m of around 145.88 °C. This endothermic can be associated to the break up of water lattices that form the secondary skeletal water layer. Since heating Ca^{2+}–Mon to 150 °C will reduce the d_{001} spacing to 1.17 nm, where, as shown in Table 1, it indicates the one water molecule layer state within the clay interlayer. Complete dehydration of Ca^{2+}–Mon interlayer can be done by heating the clay mineral to 300 °C. At this temperature, the gallery height will be reduced to d_{001} = 10.03 nm that gives the zero water molecule layer state [14].

Organically modified Ca^{2+}–Montmorillonite

Despite the big endothermic shown in Fig. 6 for Mon, thermal response of OMON shows just a small endothermic with relatively lower T_m at 36.94 °C. This observation demonstrates the intercalation effects of octadecylammonium cation which exhibits different hydration energy compared to that of Ca^{2+} cation. It thus induces new water structures that explain the reduced T_m and the loss of Mon endothermic around 150 °C. Ammonium cation with the ionic radius r = 0.143 nm [15] is a larger monovalent cation than the polyvalent Ca^{2+} cation with r = 0.099 nm [16]. These characteristics of ammonium cation contribute to its low hydration energy (84 kcal/g) compared to that of Ca^{2+} cation (410 kcal/g) as shown in Table 2 [17]. Therefore, cation exchange with the ammonium cation will reduce the amount of water content within the OMON gallery. It explains the reduced heat of fusion for the

Table 2 Hydration energy of Ca^{2+} and NH_4^+ cation

Cation*	Ionic radius, *r*/nm	Hydration energy, *U*/kcal/g*
Ca^{2+}	0.099 [14]	410
NH_4^+	0.143 [13]	84

* Barshad et al. [17]

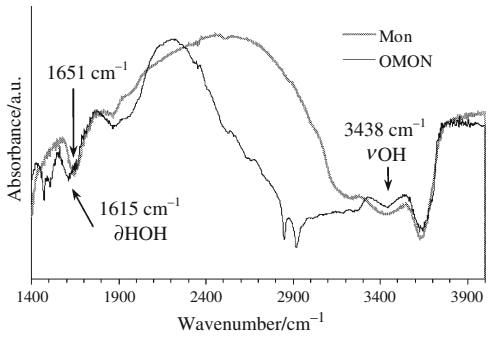

Fig. 8 FTIR spectra of Ca^{2+}–Mon and OMON show the hydroxyl bending (∂HOH) and stretching (*ν*OH) bands

OMON endothermic, to $H_{OMON} = 47.0$ J/g from $H_{Mon} = 356.3$ J/g. These observations highlight the important role of exchangeable cation to determine the water content within the Ca^{2+}–Mon gallery. More evidence is given by the FTIR spectrum in Fig. 8, where the reduced intensity of OH hydration stretching vibrations at 3,438 cm^{-1} (*ν*OH) is related to the decrease in water content within the OMON gallery. Besides, the shifting of OH band from 1,651 cm^{-1} (∂HOH) to 1,615 cm^{-1} indicates the changes in water structure within the renewed clay mineral.

ENR-50–OMON composite

Figure 9 reveals the thermal effects of OMON addition into CENR-50 composite. Although the filler content is about 30% of mass fraction, the trace of OMON as shown in Fig. 6 is absent. It shows the good interaction between ENR-50 polymer matrix and the filler domain in the composite. The interaction also altered the water structures inside the OMON gallery as revealed in Fig. 10 of the CENR-50 spectrum, where, the hydroxyl bending band (∂HOH) at 1615 cm^{-1} becomes relatively sharp and overlaps with some of ENR-50 bands. Similarly, the hydroxyl stretching band (*ν*OH) at 3438 cm^{-1} overlaps with the intermolecular hydrogen band from ENR-50 chains and is

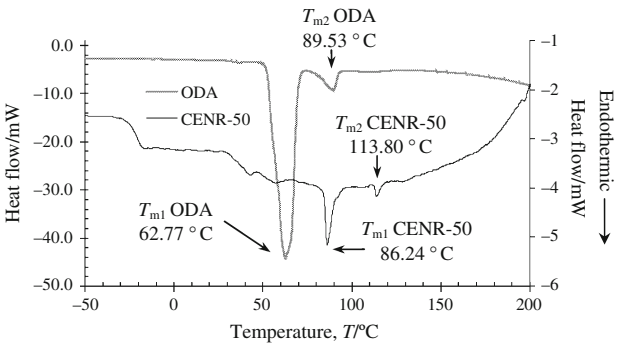

Fig. 9 DSC curves of OMON and CENR-50 composite

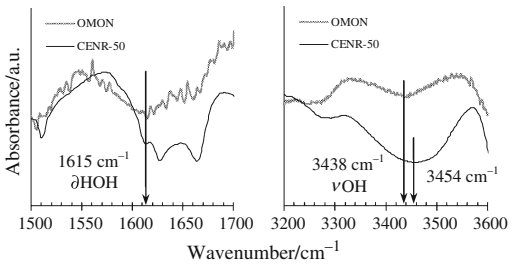

Fig. 10 FTIR spectra of OMON and CENR-50 composite show the hydroxyl bending (∂HOH) and stretching (*ν*OH) bands

shifted to 3,454 cm^{-1}. These changes explain the absence of OMON endothermic within the CENR-50 curve.

Above all, the matrix–filler interaction reveals two endothermics with their peaks of about 86.24 and 113.80 °C being assigned as T_{m1} and T_{m2}, respectively. The endothermics that resemble those from ODA demonstrate the presence of methylene chains from the alkyl ammonium cation in the OMON gallery. The shifting of T_ms toward higher temperatures could be the effect of alkyl ammonium cations interaction with the negatively charged Ca^{2+}–Mon silicate surfaces. The strong ionic interaction requires higher temperature to cause disruption on the alkyl ammonium structures. More evidence is demonstrated with the increase in heat of fusion *H* for the endothermics. Taking into consideration the mass ratio of alky ammonium component in CENR-50 composite, it gives the estimated heat of fusion $H_1 = 498.0 \pm 0.1$ J/g and $H_2 = 176.1 \pm 0.1$ J/g, which are 39–69% higher than that of ODA ($H_1 = 359.0$ J/g and $H_2 = 104.2$ J/g).

From the OMON curve in Fig. 6, only the ammonium cation effects on interlayer water can be observed while any sign of the alkyl chains are absent within $T = 20$–100 °C. However, Zidelkheir et al. [18] studies on OMON had shown the alkyl chains existence with an exothermic at 346.2 °C. This thermal response demonstrates that the alkyl chains structures were affected at higher temperature, along with the dehydroxylation on Mon silicate layers (starts above 200 °C) [19, 20] that affects their structures. In case of CENR-50, however, the thermal effects of alkyl chains can be observed within a lower temperature range (80–120 °C). The intercalation of ENR-50 chains promoted more matrix–alkyl chains interactions inside the OMON interlayer. During the DSC scan, such interactions effectively assist the heat transfer toward the alkyl chains. This condition induces thermal response from the chains, such as the T_{m1} and T_{m2} emergence, which indicate the distortions of alkyl chain structures within the relatively low temperature range. These observations thus confirm the inhabitation of the alkyl chains component from octadecyl ammonium cation inside OMON gallery, as illustrated in Fig. 11.

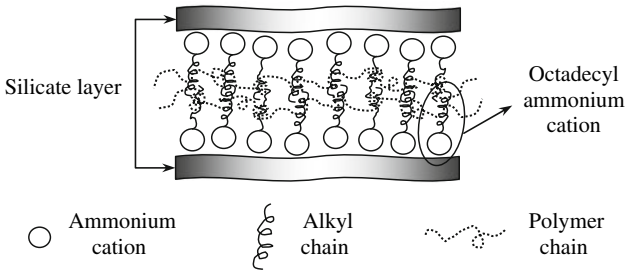

Fig. 11 Illustrations of octadecyl ammonium cations and polymeric chains intercalation within OMON interlayer space

Conclusion

Analysis on the XRD pattern reveals the structural effects of intercalation on Ca^{2+}–Mon clay mineral. DSC studies, on the other hand, show thermal behaviors of the intercalated molecules that are linked to the exchangeable cations in the clay gallery. Intercalation of water molecules within Ca^{2+}–Mon layers influences the clay mineral thermal response. From DSC profile, the Mon endothermic within the range of 20–100 °C indicates the remaoval of the free water and hydrogen bonded water molecules,. wherein, the estimated heat of fusion H_{Mon} is about 356.3 J/g with its T_m at 57.92 °C. Another Mon endothermic that gives the T_m at 150 °C demonstrates the skeletal layer disruption that forms the secondary water layer in Ca^{2+}–Mon gallery. OMON endothermic reveals the intercalation effects due to octadecyl ammonium cation. The reduced T_m at 36.94 °C and the decrease in heat of fusion ($H_{OMON} = 47.0$ J/g) indicate the changes in water structures and content, respectively, as the low hydration energy cations occupy the modified clay gallery. The penetration of ENR-50 chains into OMON interlayer facilitates the heat transfer onto the intercalated modifier cations. Two endothermics at $T_{m1} = 86.24$ °C and $T_{m2} = 113.80$ °C show the thermal effects of alkyl component on the octadecyl ammonium cation. The relatively higher heat of fusion $H_1 = 498.0$ J/g and $H_2 = 176.1$ J/g compared to that of ODA is caused by the strong ionic interaction between the cation and the negatively charged Mon surface. The findings from the studies thus prove that the modifier cation intercalation locates both ammonium cation and the alkyl chain segment inside the OMON gallery.

References

1. Theng BKG. Formation and properties of clay–polymer complexes. Amsterdam: Elsevier; 1979.
2. Grim RE. Clay mineralogy. 2nd ed. New York: McGraw-Hill; 1968.
3. Fusova L. Modification of the structure of Ca–montmorillonite. GeoSci Eng. 2009;IV(1):27–32.
4. Mering J. On the hydration of montmorillonite. Trans Faraday Soc. 1946;42B:205–19.
5. Janowska G, Mikolajczyk T, Olejnik M. Effect of montmorillonite content and the type of its modifier on the thermal properties and flammability of polyimideamide nanocomposite fibers. J Therm Anal Calorim. 2008;92:495–503.
6. Lin HL, Chang HL, Juang TY, Lee RH, Dai SA, Liu YL, Jeng RJ. Nonlinear optical, poly(amide-imide)–clay nanocomposites comprising an azobenzene moiety synthesised via sequential self-repetitive reaction. Dyes Pigments. 2009;82:76–83.
7. Pavlidou S, Papaspyrides CD. A review on polymer-layered silicate nanocomposites. Prog Poly Sci. 2008;33:1119–98.
8. Román F, Montserrat S, Hutchinson JM. On the effect of montmorillonite in curing reaction of epoxy nanocomposites. J Therm Anal Calorim. 2007;87:113–8.
9. Peila R, Lengvinaite S, Malucelli G, Priola A, Ronchetti S. Modified organophilic montmorillonite/LDPE nanocomposites. J Therm Anal Calorim. 2008;91:107–11.
10. Zhao Z, Yu W, Liu Y, Zhang J, Shao Z. Isothermal crystallization behaviors of nylon 6 and nylon 6/montmorillonite nanocomposite. Mater Lett. 2004;58:802–6.
11. Yasuniwa M, Tsubakihara S, Fujioka T. X-ray and DSC studies on the melt-recrystallization process of poly(butylene naphthalate). Thermochim Acta. 2003;396:75–8.
12. Ganguly S, Dana K, Ghatak S. Thermogravimetric study of n-alkylammonium-intercalated montmorillonites of different cation exchange capacity. J Therm Anal Calorim. 2009; doi: 10.1007/s10973-009-0588-0.
13. Tsuchiya M, Kojima T. The double endothermic phenomenon of polytetra-hydrofurans in the melting temperature region. J Therm Anal Calorim. 2005;80:159–62.
14. Bray HJ, Redfern SAT, Clark SM. The kinetic of dehydration in Ca-montmorillonite: an in situ X-ray diffraction study. Mineral Meg. 1998;62(5):647–56.
15. Jorgensen TC, Weatherley LR. Ammonia removal from wastewater by ion exchange in the present of organic contaminants. Water Res. 2003;37:1723–8.
16. Lal R. Encyclopedia of soil science, vol. 1. Boca Raton: CRC Press–Taylor & Francis Group; 2006.
17. Barshad I. Factor affecting the interlayer expansion of vermiculite and montmorillonite with organic substances. Soil Sci Soc Proc. 1952;16:176–82.
18. Zidelkheir B, Abdelgoad M. Effect of surfactant agent upon the structure of montmorillonite: X-ray diffraction and thermal analysis. J Therm Anal Calorim. 2008;94:181–7.
19. Bala P, Samantaray BK, Srivastava SK. Dehydration transformation in Ca-montmorillonite. Bull Mater Sci. 2000;23(1):61–7.
20. Bray HJ, Redfern SAT. Kinetic of dehydration of Ca-montmorillonite. Phys Chem Minerals. 1999;26:591–600.